

Direct Measurement of Focusing Fields in Active Plasma Lenses

J.-H. Röckemann¹, L. Schaper¹, S. K. Barber², N. A. Bobrova³, G. Boyle¹, S. Bulanov², N. Delbos^{4,6}, K. Floettmann¹, G. Kube¹, W. Lauth², W. P. Leemans², V. Libov^{1,6}, A. Maier^{4,6}, M. Meisel^{1,6}, P. Messner^{4,6}, P. V. Sasorov³, C. B. Schroeder², J. van Tilborg², S. Wesch¹, and J. Osterhoff^{*1}

¹Deutsches Elektronen-Synchrotron DESY, Notkestraße 85, 22607 Hamburg, Germany

²Lawrence Berkeley National Laboratory, University of California, Berkeley, California 94720, USA

³Keldysh Institute for Applied Mathematics, Moscow 125047, Russia

⁴Center for Free-Electron Laser Science and Department of Physics, Luruper Chaussee 149, 22761 Hamburg, Germany

⁵Johannes Gutenberg-Universität Mainz, Saarstraße 21, 55122 Mainz, Germany

⁶Universität Hamburg, Mittelweg 177, 20148 Hamburg, Germany

December 3, 2024

Abstract

Active plasma lenses have the potential to enable broad-ranging applications of plasma-based accelerators owing to their compact design and radially symmetric kT/m-level focusing fields, facilitating beam-quality preservation and compact beam transport. We report on the direct measurement of magnetic field gradients in active plasma lenses and demonstrate their impact on the emittance of a charged particle beam. This is made possible by the use of a well-characterized electron beam with 1.4 mm mrad normalized emittance from a conventional accelerator. Field gradients of up to 823 T/m are investigated. The observed emittance evolution is supported by numerical simulations, which demonstrate the conservation of the core beam emittance in such a plasma lens setup.

*corresponding author: jens.osterhoff@desy.de

Laser wakefield accelerators (LWFAs) allow for the generation of extreme electric fields on the order of 100 GV/m for charged particle acceleration and can deliver beams of sub- μm normalized emittance [1, 2], multi-kA peak currents [3], and femtosecond pulse duration [4, 5, 6]. LWFAs have shown the capability to produce multi-GeV electron beams in cm-scale structures [7, 8, 9]. Their application to drive compact sources of coherent X-ray beams [10, 11] and incoherent MeV photons [12], ultra-fast electron diffraction experiments [13, 14], and high-energy particle colliders [15] has been proposed and studied [16, 17]. For all these applications small beam emittances are critical. Indeed, beams from plasma accelerators are susceptible to chromatic emittance growth in the drift following the acceleration section [18, 19]. Thus, beam capturing within a few centimeters after the plasma exit is crucial for emittance preservation.

In this context, conventional focusing optics face problems: Solenoids suffer from large chromaticity and weak focusing for relativistic beams owing to their $1/\gamma^2$ -scaling of the focusing strength, with the relativistic Lorentz factor γ . The more favorable $1/\gamma$ -scaling in combination with high field gradients ($\sim 500\text{ T/m}$ for permanent magnets) of quadrupoles is put into perspective when considering that two quadrupoles need to be combined to achieve focusing in both transverse planes. Hence, quadrupoles, which are inherently defocusing in one plane, increase chromatic emittance growth in this plane dramatically [20].

Active plasma lenses [21] (APLs) potentially offer an elegant solution with their compact size, azimuthally symmetric focusing, and high magnetic field gradients, which have been shown to exceed 3 kT/m [22]. Recent studies indicate that nonuniform current densities may form inside discharge capillary based APLs [23, 24, 25, 26, 27], leading to nonlinear magnetic field gradients and, subsequently, emittance deterioration [28, 29]. In this work we report on a first direct measurement of the magnetic field distribution inside an APL and complement these results by experimentally detecting its influence on the emittance of a stable, well-characterized electron beam from a conventional accelerator. These studies are supported by simulations and show the potential for emittance preservation.

Active plasma lenses for electron beams typically consist of a gas-filled capillary with a circular cross-section of mm-scale diameter and cm-scale length machined into glass or sapphire. A multi-kV discharge voltage is applied to the capillary ends, leading to breakdown of the gas. Subsequently, a current is driven along the generated plasma column forming an azimuthal magnetic field. In the following, we assume a azimuthally symmetric current distribution $J(r)$, with r denoting the radial position. Ampere's law provides the cylindrically symmetric magnetic field

$$B_\phi(r) \cdot r = \mu_0 \int_0^r J(r') r' dr', \quad (1)$$

for $r < R$, with R being the capillary radius and μ_0 the vacuum permeability. The magnetic field distribution becomes $B_{\phi,\text{ideal}}(r) = \mu_0 I_0 r / (2\pi R^2)$ in case of a uniform current distribution $J = I_0 / (\pi R^2)$, with I_0 being the total current. Differentiating this expression yields the ideal magnetic field gradient

$$g_{\text{ideal}} = \mu_0 I_0 / (2\pi R^2). \quad (2)$$

In general, Eq. (2) does not hold since the current distribution homogeneity $J(r)$ is not uniform. A transverse temperature gradient forms due to cooling of the

plasma at the capillary wall leading to a radially changing Ohmic resistance, a nonuniform current distribution, and a nonlinear magnetic field gradient. Fig. 1 shows the result of a one-dimensional magnetohydrodynamic (MHD) simulation of a capillary of $R = 0.5$ mm radius filled with hydrogen of $n_0 = 10^{17} \text{ cm}^{-3}$ molecular density traversed by a current of $I_0 = 364$ A assuming a fixed electron temperature at the wall interface of $T^* = 0.5$ eV. The radial position is normalized to R , the magnetic field to B_{ideal} . Cases with $I_0 = 188$ A, and 740 A have also been simulated. The MHD modeling shows that for the currents used, the fraction of ionized hydrogen was well above 80%.

An analytic model for the current distribution in a plasma lens was introduced in [28]. It is based on the Spitzer collisional model of plasma, in which the conductivity σ depends on the plasma density n_e and electron temperature T_e via

$$\sigma = \frac{32\epsilon_0^2}{\ln\Lambda} \cdot \frac{(k_B T_e)^{3/2}}{e^2 m_e^{1/2}}, \quad (3)$$

with $\lambda_D = \sqrt{\epsilon_0 k_B T_e / n_e e^2}$, $\Lambda = n_e \lambda_D^3$, k_B the Boltzmann constant, ϵ_0 the vacuum permittivity, e the electron charge, and m_e the electron mass. The scaling of σ is dominated by T_e since n_e appears only logarithmic in Λ . Thus, the current density is dominated by the temperature $J(r) = \sigma E \sim T_e^{3/2}$. Following the work of [23, 28], the temperature distribution satisfies the heat flow equation

$$\frac{1}{x} \frac{d}{dx} \left(x \frac{du}{dx} \right) = -u^{3/7}, \quad (4)$$

in which $u^{2/7} = T_e/A$ with $A = (7\sigma_0 R^2 E^2 / 2\kappa_0)^{1/2}$, $x = r/R$, and the thermal and electric conductivities were assumed to scale with $\kappa = \kappa_0 T_e^{5/2}$ and $\sigma = \sigma_0 T_e^{3/2}$, respectively. The boundary conditions satisfy $dT_e(x=0)/dx = 0$ and $T_e(x=1) = T^*$ with T^* the temperature at the wall. The current distribution can be expressed as

$$J(r) = \frac{I_0 u(r)^{3/7}}{2\pi R^2 m_I}, \quad (5)$$

with $m_I = \int_0^1 u^{3/7} x dx$. The central region $x < 1$ can be written as

$$J(r) = \frac{I_0}{\pi R^2} \left(\frac{u(0)^{3/7}}{2m_I} \right) \left[1 - \frac{3}{28} u(0)^{-4/7} x^2 - \frac{15}{3136} u(0)^{-8/7} x^4 \right], \quad (6)$$

and

$$B_\phi(x) = \frac{\mu_0 I_0}{2\pi R} \cdot \frac{u(0)^{3/7}}{2m_I} \cdot x \cdot \left[1 - \frac{3}{56} u(0)^{-4/7} x^2 - \frac{5}{3136} u(0)^{-8/7} x^4 \right]. \quad (7)$$

An important figure of merit for the linearity of an APL is its core linear magnetic field slope in comparison to the ideal magnetic field slope, defined as $\Delta g = g_{\text{core}}/g_{\text{ideal}} = \frac{u(0)^{3/7}}{2m_I}$. The Δg -factor for the $J \sim T^{3/2}$ -model in Fig. 1 is $\Delta g = 1.48$. This corresponds to a cold wall boundary condition. The corresponding gradients are given in Tab. 1. R and I_0 were measured with high precision ($\sim 1\%$) in this experiment, such that a measurement of the gradient in the central region of the

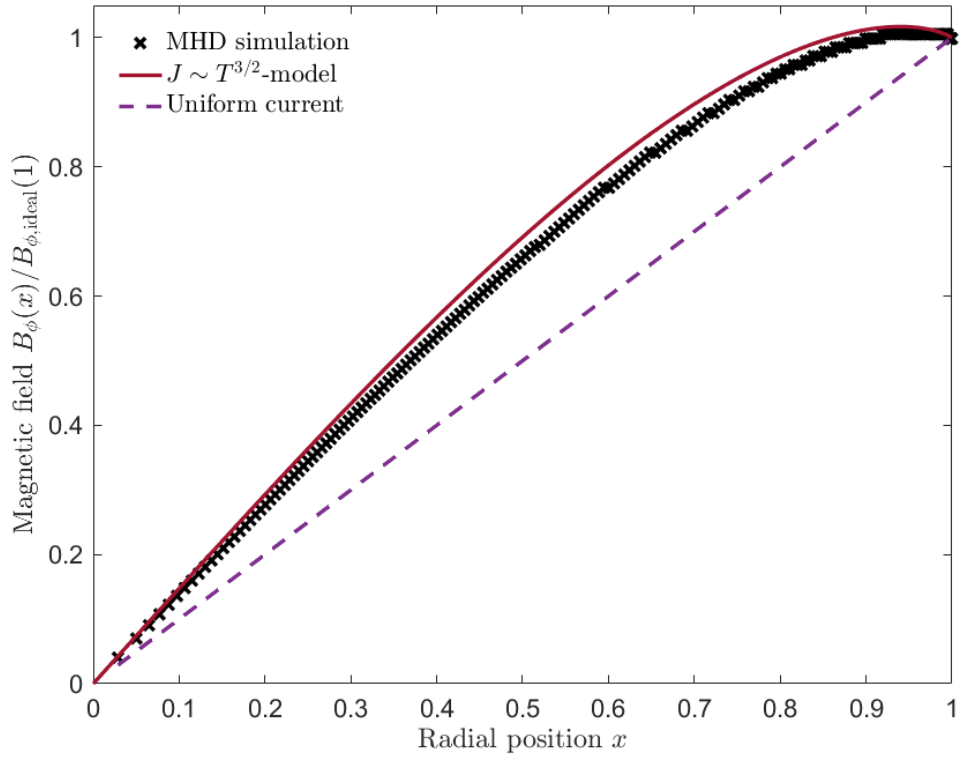


Figure 1: MHD simulation results for a $R = 0.5$ mm gas column with $I_0 = 364$ A. The $J \sim T^{3/2}$ -model is of the form of Eq. (7).

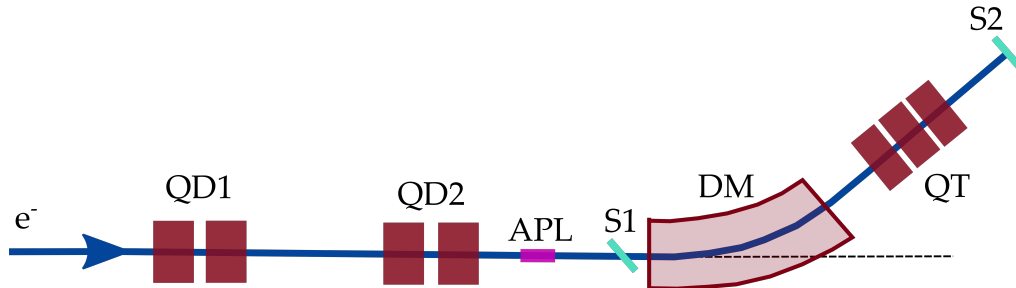


Figure 2: Schematic of the accelerator beamline at MaMi-B. QD1: first quadrupole duplet; QD2: second quadrupole duplet; APL: active plasma lens; S1: screen used in the offset measurements; DM: dipole magnet; QT: quadrupole triplet used in the emittance measurements; S2: screen used in the emittance measurements.

APL provides a means of assessing the magnetic field distribution for the entire capillary diameter via the $J \sim T^{3/2}$ -model.

A race-track Microtron at the university of Mainz, the Mainz Microtron B (MaMi-B), was used for probing the magnetic field of an APL. MaMi-B was operated in a mode in which it delivered 10 ns long bunches with an average current of 100 μA , an energy of 855 MeV, and a normalized vertical emittance of $\epsilon_i = 1.37 \pm 0.01 \mu\text{m rad}$. The APL itself consisted of a 7 mm long capillary of $R = 0.5 \text{ mm}$ machined into a sapphire block. A continuous flow of hydrogen was supplied to the capillary at 4 mbar backing pressure through two inlets of $R = 0.75 \text{ mm}$ diameter situated 1.5 mm from the capillary ends leading to a molecular density of $n_0 = 10^{17} \text{ cm}^{-3}$ inside the capillary. Copper electrodes on both sides connected a pulse-forming network [30] to the gas volume. A discharge voltage of 9 kV - 20 kV was applied which resulted in stable flat-top currents of 188 A - 740 A arising 100 ns after the discharge trigger for a duration of 240 ns. The electron beam traversed the APL 100 ns after the current plateaued. A schematic drawing of the beamline can be found in Fig. 2.

Direct measurements of the APL magnetic field gradients were performed by introducing a transverse offset of the APL with respect to the electron beam position, thus introducing a dipole kick to the beam. The centroid shift of the MaMi-B beam $d = 25.3 \text{ cm}$ downstream of the APL was measured and averaged over 100 shots per offset. The results can be seen in Fig. 3. The formation of fringe fields was discussed in [31]. The influence of these fields on the emittance of a

passing MaMi-type beam was simulated in ASTRA [32] and found to be negligible on the sub-percent level. The longitudinal current ramp in the fringe fields was modeled after $I(z_{\text{edge}}) = I_0/(1 + \exp(4z_{\text{edge}}/\sigma_{\text{ramp}}))$, where z_{edge} is the distance from the capillary end and σ_{ramp} is the ramp taper parameter, as commonly used in conventional magnet optics. Owing to the fringe fields, the effective magnetic length $L = L_{\text{capillary}} + 2 \cdot L_{\text{fringe}}$ of the APL extends beyond the sapphire capillary itself. So the beam offset $\Delta\langle x \rangle$ is dependent on the lens offset r and effective length L through the magnetic field like

$$\Delta\langle x \rangle = \frac{q \cdot d}{p} \int_0^L B_\phi(r) z dz, \quad (8)$$

in which p is the particle momentum, q its charge. To account for the additional uncertainty owing to the fringe field, the data in Fig. 3 was fitted for the range of $L_{\text{fringe}} \leq 0.5$ mm (which is well above the length found in [31]). The derived core gradients g_{core} for $L_{\text{fringe}} = 0.25$ mm including the systematic uncertainty for $L_{\text{fringe}} \leq 0.5$ mm can be found in Tab. 1. The obtained magnetic field gradients are in good agreement with a $J \sim T^{3/2}$ -model assuming a cold wall boundary condition. It is noteworthy that the relative center-of-mass jitter of the MaMi-B beam was not affected by the APL even for the extreme case of 350 μm offset. This means the magnetic field in the APL was highly reproducible, which may also be seen in the small error bars of the measured beam position in Fig. 3. Fig. 4 shows the derived values from the offset scan and as an additional data point the magnetic field at $r = R$ derived from the R and I_0 measurements. Additionally the predicted behavior from the $J \sim T^{3/2}$ -model assuming a cold wall boundary condition are shown.

A complementary way of probing the nonlinearity of the magnetic field in the APL is measuring the emittance change of an electron beam after passage through the APL. Quadrupole scans were performed for different plasma lens settings in order to detect emittance change due to nonlinear field gradients. The currents used in the experiment were 188, 364, and 740 A. The current amplitude had a jitter of 1.5 A rms in each case. This measurement technique requires the beamline upstream of the quadrupoles used for the scan to be stable. The APL stability greatly facilitated these emittance measurements and is reflected in the relatively low rms beam size variation during the scans of $< 5\%$ (100 shots were averaged per setting). An rms beam size of $\sigma_y = 154_{-15}^{+5}$ μm vertically and $\sigma_x = 151_{-12}^{+2}$ μm horizontally and a small divergence $\sigma_{x',y'} < 0.1$ mrad was used at the APL entrance to sample over a wide range of the magnetic field. The results of three quadrupole scans are shown in Tab. 1. The measured beam sizes including fits can be found in Fig. 5. The optical system had a resolution of 20 μm which was well suited for the 45 μm of minimal beam size used in the scans.

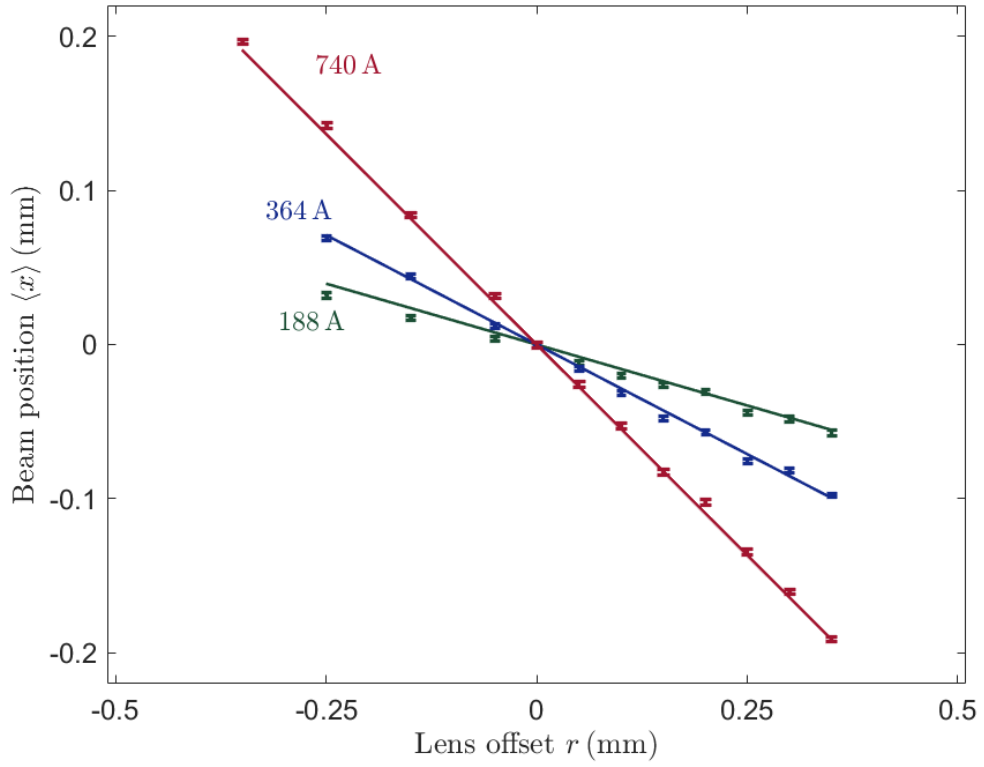


Figure 3: Results from offset scan using $I_0 = 188$ A, 364 A and 740 A of total current. The lines are linear fits to the data.

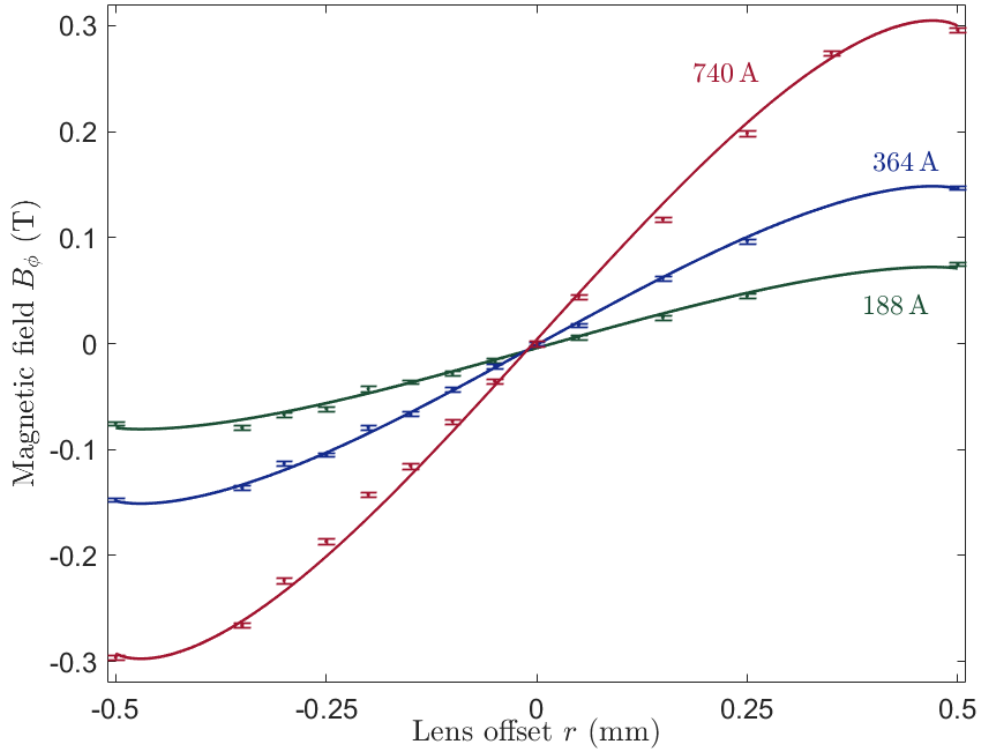


Figure 4: Magnetic field strength derived from the offset scan data in Fig. 3 and measurements of R and I_0 with an $L = 7.5$ mm APL. The lines show the predicted behavior from the $J \sim T^{3/2}$ -model.

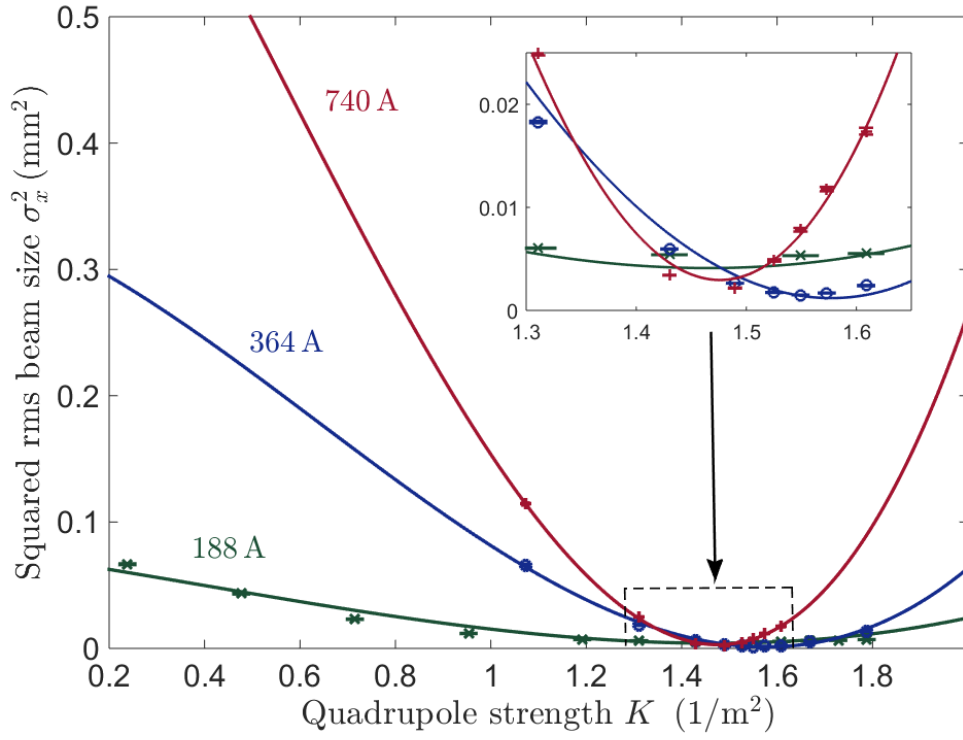


Figure 5: Quadrupole scan results for the APL operated at 188 A, 364 A, and 740 A of total current. Error bars for beam size measurements are included. The fitted emittances can be found in Tab. 1.

Table 1: Comparison of measured and simulated gradients and emittances. The measured gradients are calculated for an effective length of $L = 7.5$ mm. Additionally, systematic uncertainties arising from the fringe fields are given. The emittance was simulated for $\sigma = 154 \mu\text{m}$ and a field in the form of the $J \sim T^{3/2}$ -model (cf. Fig. 1).

I_0 (A)	g_{core} (T/m)			ϵ_f (mm mrad)	
	Meas.	Fringe	$J \sim T^{3/2}$	Meas.	Sim.
188	238 ± 9	± 17	223	2.2 ± 0.1	2.5
364	428 ± 6	± 30	431	3.7 ± 0.1	4.3
740	823 ± 8	± 59	876	8.2 ± 0.1	8.4

The emittance growth in an $L = 7.5$ mm long APL was simulated with the particle tracking code ASTRA. The field was modeled to be of the form given by the $J \sim T^{3/2}$ -model. Transversally Gaussian shaped beams with rms beam size of $\sigma_{x,y} = 154 \mu\text{m}$ were assumed for the simulation. This corresponds to the rms beam size measured 25.3 cm downstream of the APL with the APL turned off. The measurements and simulation results are in good agreement. They suggest a smaller beam size in the APL than used here is favorable to minimize emittance growth. Fig. 6 shows particle tracking simulation results for different incoming rms beam sizes traversing the magnetic field distributions obtained from the $J \sim T^{3/2}$ -model and $L = 7.5$ mm. The emittance growth is highly dependent on the incoming beam size and can be eliminated for beams with $\sigma < 75 \mu\text{m}$ on the 1 mm mrad normalized emittance scale.

In summary, magnetic field gradients of a 1-mm diameter plasma lens and emittance change due to nonlinear focusing fields have been measured directly using the conventional accelerator Mainz Microtron. We observed excellent gradient stability. The measured gradient increase showed the predicted behavior compared to the uniform current density case for a cold wall boundary condition $J \sim T^{3/2}$ -model. The measured emittance change of a passing electron beam agrees with predictions made by magnetohydrodynamics simulations, direct gradient measurements and particle tracking simulations. We showed in simulations that using beams with an rms size smaller than 20% of the APL radius leads to emittance preservation on the $\mu\text{m rad}$ -level. Future studies will focus on mitigating emittance degradation further by manipulating the current density behavior in the APL by using different gas species and optimizing radii and total currents used.

We acknowledge the support through the Helmholtz Virtual Institute VH-VI-503, the Helmholtz Matter and Technologies Accelerator Research and Development program, the Helmholtz IuVF ZT-0009 program, and the U.S. Dept. of Energy under contract No. DE-AC02-05CH11231.

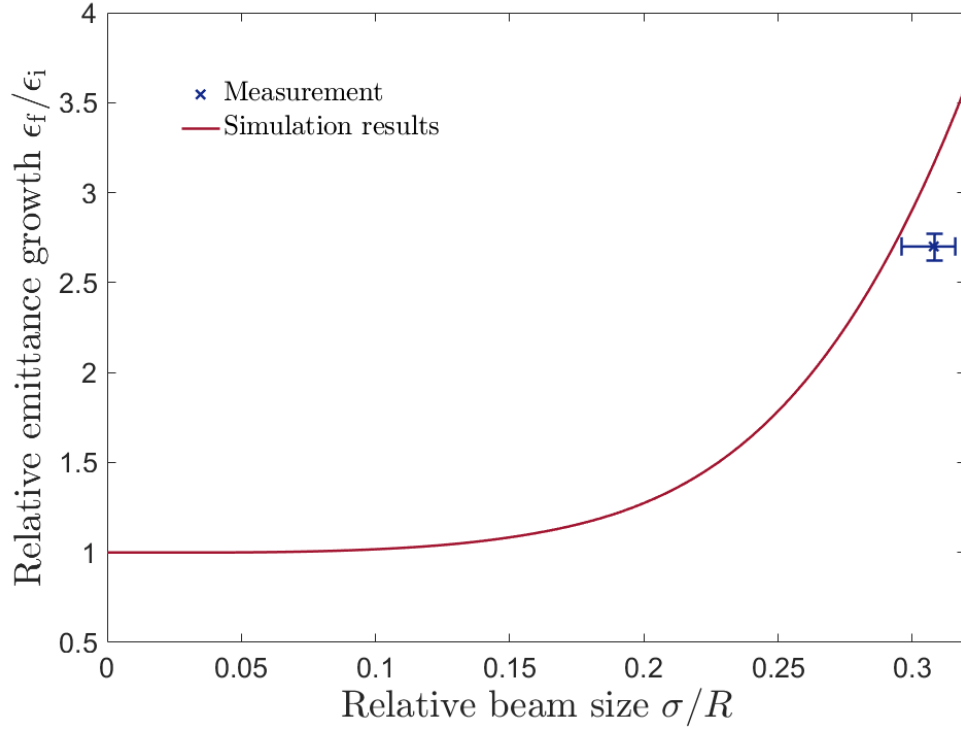


Figure 6: Particle tracking simulation results for relative emittance degradation of a MaMi-like beam in dependence of incoming rms beam size for an APL with $R = 0.5$ mm and $I_0 = 364$ A. The measured emittance degradation for this setup is also shown.

References

- [1] S. Barber, *et al.*, *Phys. Rev. Lett.* **119**, 104801 (2017).
- [2] R. Weingartner, *et al.*, *Physical Review Accelerators and Beams* **15**, 111302 (2012).
- [3] C. Geddes, C. Toth, J. van Tilborg, E. Esarey, *et al.*, *Nature* **431**, 538 (2004).
- [4] O. Lundh, *et al.*, *Nature Physics* **7**, 219 (2011).
- [5] K. Zeil, *et al.*, *Nature Communications* **3**, 219 (2012).
- [6] A. Buck, *et al.*, *Nature Physics* **7**, 543 (2011).
- [7] H. T. Kim, *et al.*, *Physical Review Letters* **111**, 165002 (2013).
- [8] X. Wang, *et al.*, *Nature Communications* **4** (2013).
- [9] W. Leemans, *et al.*, *Physical Review Letters* **113**, 245002 (2014).
- [10] A. Maier, *et al.*, *Physical Review X* **2**, 031019 (2012).
- [11] Z. Huang, Y. Ding, C. B. Schroeder, *Physical Review Letters* **109**, 204801 (2012).
- [12] S. Chen, *et al.*, *Physical Review letters* **110**, 155003 (2013).
- [13] P. Catravas, *et al.*, *Meas. Sci. Technol.* **12**, 1828 (2001).
- [14] F. Hartemann, *et al.*, *IEEE Transactions on Nuclear Science* **10**, 011301 (2007).
- [15] C. Schroeder, E. Esarey, C. Geddes, C. Benedetti, W. Leemans, *Physical Review Special Topics-Accelerators and Beams* **13**, 101301 (2010).
- [16] Y. Glinec, *et al.*, *Physical Review Letters* **94**, 025003 (2005).
- [17] N. D. Powers, *et al.*, *Nature Photonics* **8**, 28 (2014).
- [18] K. Floettmann, *Physical Review Special Topics-Accelerators and Beams* **6**, 034202 (2003).
- [19] T. Mehrling, J. Grebenyuk, F. Tsung, K. Floettmann, J. Osterhoff, *Physical Review Special Topics-Accelerators and Beams* **15**, 111303 (2012).
- [20] C. Lindstrøm, E. Adli, *Physical Review Special Topics-Accelerators and Beams* **19**, 071002 (2016).
- [21] E. Forsyth, *et al.*, *Meas. Sci. Technol.* **12**, 872 (1965).
- [22] J. van Tilborg, *et al.*, *Physical Review Letters* **115**, 184802 (2015).
- [23] N. Bobrova, *et al.*, *Physical Review E* **65**, 016407 (2001).

- [24] D. Spence, S. M. Hooker, *Physical Review E* **63**, 015401 (2000).
- [25] A. Butler, D. Spence, S. M. Hooker, *Physical Review Letters* **89**, 185003 (2002).
- [26] C. McGuffey, *et al.*, *Physics of Plasmas* **16**, 113105 (2009).
- [27] A. Gonsalves, *et al.*, *Journal of Applied Physics* **119**, 033302 (2016).
- [28] J. van Tilborg, *et al.*, *Physical Review Accelerators and Beams* **20**, 032803 (2017).
- [29] R. Pompili, *et al.*, *Applied Physics Letters* **110**, 104101 (2017).
- [30] P. G. Donald, Pulse forming network (1956). US Patent 2,769,903.
- [31] G. Bagdasarov, *et al.*, *Physics of Plasmas* **24**, 083109 (2017).
- [32] K. Floettmann, Astra particle tracking code. www.desy.de/~mpyflo.